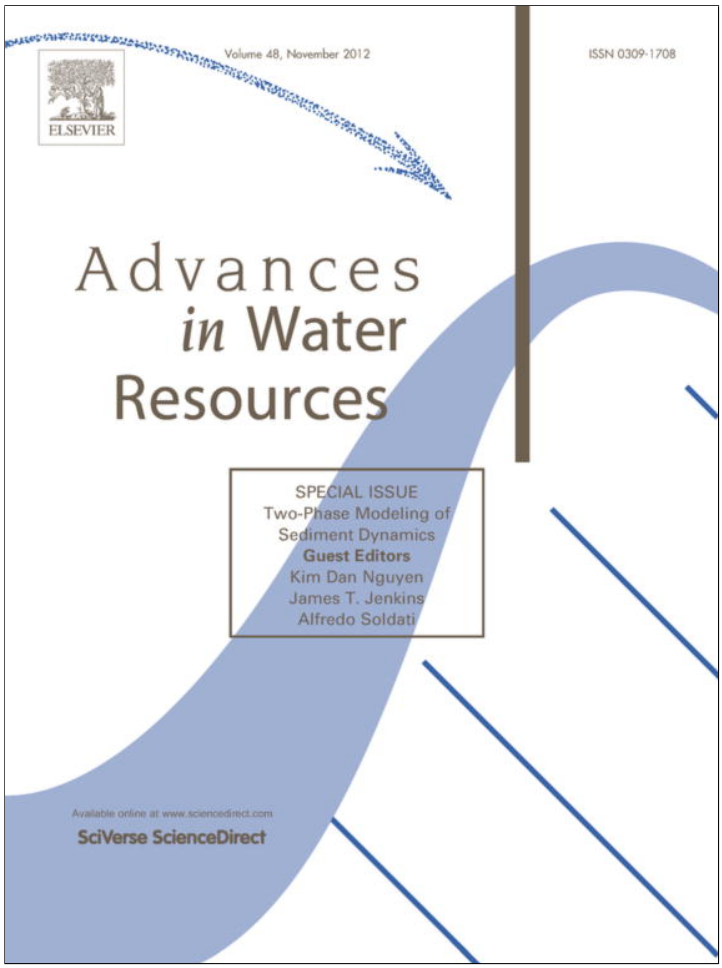

Advances in Water Resources 48 (2012) 18–30

Contents lists available at SciVerse ScienceDirect

Advances in Water Resources

journal homepage: www.elsevier.com/locate/advwatres

Sediment transport in steady turbulent boundary layers: Potentials, limitations, and perspectives for Lagrangian tracking in DNS and LES

Alfredo Soldati *, Cristian Marchioli

Department of Fluid Mechanics, International Centre for Mechanical Sciences, 33100 Udine, Italy
Centro Interdipartimentale di Fluidodinamica e Idraulica, Università di Udine, Udine 33100, Italy

ARTICLE INFO

Article history:
Available online 30 May 2012

Keywords:
Sediment suspension
Turbulent boundary layer
Direct numerical simulation
Large-eddy simulation
Particle tracking
Modelling

ABSTRACT

In this paper, we discuss the applicability of the Eulerian–Lagrangian point-particle approach to predict sedimentation and resuspension phenomena in solid–liquid flows. We start from results obtained for dilute systems and we examine to which degree such results can be applied to sedimentation phenomena, in which higher concentration values will be at some point relevant. We examine critical issues in state-of-the-art direct and large-eddy simulations of sediment dynamics in turbulence, starting from concepts and ideas that were derived from a systematic study of particle transport in turbulent boundary layer and applied to several canonical flow configurations (closed/open channel with flat/wavy bottom). We focus on issues related to high sediment concentration near the boundary and we examine critically results from original modelling strategies specifically aimed at dealing with boundary conditions where concentration peaks, with inter-particle collisions and with subgrid scale models in higher Reynolds number simulations employing LES.

1. Introduction

Current state of the art in direct numerical simulation (DNS) and large-eddy simulation (LES) with Lagrangian tracking (LPT) of pointwise particles is mature enough to ensure comprehension of crucial two-phase flow phenomena such as preferential concentration, deposition and re-entrainment [1]. In the specific context of sediment suspensions, today challenges are represented by boundary conditions (to reproduce particle–wall interactions), particle interaction kernels (to model collisions and/or fluid-particle interplay) and local phenomena occurring close to the boundaries (to predict particle accumulation rates). These features control particle transport and distribution within the flow, especially in regions with large mean gradients and low mean velocities (e.g. boundaries), and have a major impact in many applications. Examples include separation and purification processes in ducts and pipes [2], pneumatic conveying [3], and sedimentation of sand-like particles in turbulent water flows [4]. The macroscopic behavior of these two-phase systems is further influenced by inertia, which however plays a role at the microscale of a single sediment particle: an inertial particle acts as a low-pass filter for high frequency turbulence fluctuations with a response fully established by the pattern of coherent fluid motions [5,6]. Inertial bias produces preferential concentration of sediments and determines transfer rates by inducing deposition or resuspension fluxes. In turn, these fluxes control vertical mixing and drive the formation of complex bedforms such as dunes and ripples in environmental flows [7,8].

Preferential concentration effects may limit the predictive capability of point-particle DNS, particularly when associated with strong concentration gradients and locally high mass/volume fractions [9]. These conditions are often found in sediment transport problems: one example of such limitation is provided in Fig. 1 for the case of horizontal turbulent flow in shallow open channel at shear Reynolds number $Re_\tau = 85.5$ and Froude number $Fr = 4.06$ [10] (see Section 2 for definitions). In this figure, vertical mixing is quantified by the sediment concentration in the direction perpendicular to the mean flow. Sediment particles are characterized by specific density $S \simeq 2$ (sand particles in water) and Stokes number $St = 0.5$. The Stokes number is defined as $St = \tau_p/\tau_f$ where $\tau_p = \rho_p d_p^2/18\mu$ is the characteristic time of a particle with density ρ_p and diameter d_p moving in a fluid with dynamic viscosity μ, and $\tau_f = \mu/\langle\tau_w\rangle$ is the flow characteristic time scale, with $\langle\tau_w\rangle$ the mean shear stress at the wall. The vertical coordinate is given in dimensionless form as $z^+ = z\sqrt{\rho\langle\tau_w\rangle/\mu^2}$ with ρ the fluid density. Plotted data (symbols) were generated performing LPT of $\mathcal{O}(10^5)$ individual sediment particles in DNS fields and assuming dilute flow conditions (which imply one-way coupling and neglecting particle–particle interactions) [10]. In Fig. 1 we also plot the Rouse profile [11]:

* Corresponding author at: Centro Interdipartimentale di Fluidodinamica e Idraulica, Università di Udine, Udine 33100, Italy.
E-mail addresses: soldati@uniud.it (A. Soldati), marchioli@uniud.it (C. Marchioli).

0309-1708/$ - see front matter © 2012 Elsevier Ltd. All rights reserved.
http://dx.doi.org/10.1016/j.advwatres.2012.05.011

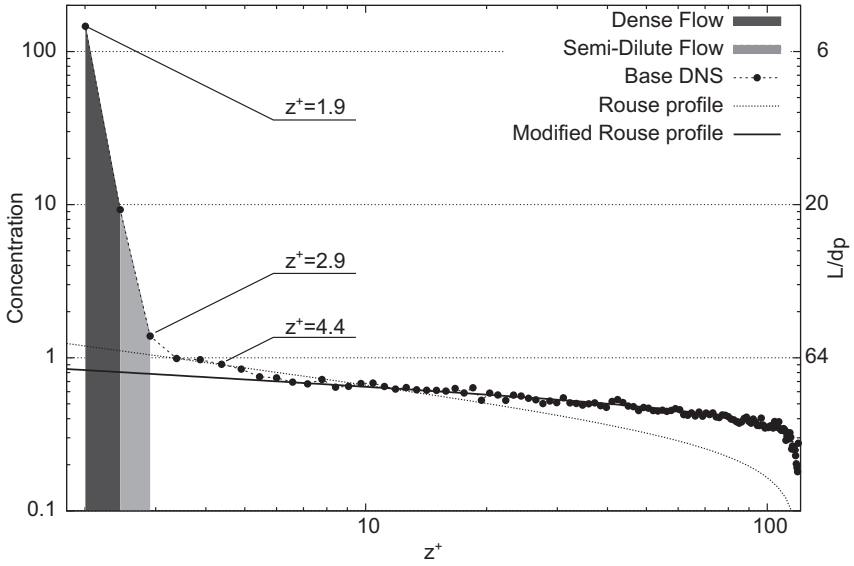

Fig. 1. Vertical mixing of sediment particles ($St = 0.5$) in turbulent boundary layer ($Re_\tau = 85.5$): comparison of numerical concentration profiles from point-particle DNS (symbols) against Rouse model prediction (dashed line) and modified Rouse model prediction (solid line).

$$C(z) = C_{ref}\left[\frac{(h-z)z}{(h-z_{ref})z_{ref}}\right]^{\beta}, \tag{1}$$

where C_{ref} is a reference concentration measured at distance z_{ref} from the wall, while $\beta = v_s/ku_\tau$ is the correction coefficient, with v_s the terminal velocity of a particle moving in still fluid subject to drag and gravity only, $k \simeq 0.41$ the von Kármán constant, and $u_\tau = \sqrt{\langle\tau_w\rangle/\rho}$ the shear velocity. The Rouse profile provides an estimate of sediment concentration in steady, uniform flow under the assumption that the turbulent concentration flux can be reproduced by an isotropic eddy viscosity model. We remark here that Eq. (1) has been validated experimentally for low sediment concentration and small particle size. In Fig. 1, we chose $z^+_{ref} = 3.38$, corresponding to roughly two particle diameters from the wall ($z_{ref}/H \simeq 0.04$), and $C_{ref} = 1$. We consider two different values of β. The value for β obtained through the definition given above is $\beta = 0.35$, and provides a poor approximation for the present sediment distribution (dotted line). This might be due to inadequacies in the methodology, but also to the strong assumptions at the basis of Eq. (1) [12,13]. To improve the prediction of Eq. (1) we optimized the value of β over our DNS data (similar to Chan-Braun et al. [13]) and we obtained $\beta_{mod} = 0.57\beta$. This value leads to a remarkable fit with the present DNS data, yet only for $z/H \geqslant 0.03$ (solid line). Similar results have been obtained by Widera et al. [7] for pointwise sediments suspended in horizontal wavy channel and by Chan-Braun et al. [13] considering interface-resolved sediment transport in horizontal open channel, confirming that good agreement between numerical results and the Rouse profile can hardly be found all the way to the boundary.

The concentration profile shown in Fig. 1 is evolving with time and, at the instant captured in the figure (still far from equilibrium [14]), it is developing a growing maximum well into the near-wall region ($0 < z^+ < 3$). This behavior can be viewed as the consequence of the turbulence non-homogeneity, and has been observed in a number of previous works (see [5] and references therein). The near-wall peak of concentration is associated with regions of semi-dilute flow where two-way coupling effects due to sediments back-reacting on the flow become significant: these regions, identified by the light-grey area in Fig. 1, are characterized by inter-particle spacing $L/d_p = (\pi/6\alpha_p)^{1/3} > 10$, where α_p is the volume fraction of point-particles at relative distance L. With oscillatory boundary layers, such regions may be characterized by the occurrence of significant concentration gradients due to particle-induced density stratification effects [15,16]. The peak is also associated with regions of dense flow (resembling those typical of sheet flow layers [17]) where modelling four-way coupling effects due to inter-particle collisions becomes inevitably necessary. These regions are identified by the dark-grey area in Fig. 1, and are characterized by $1 < L/d_p < 10$. In both cases, the one-way coupling assumption breaks down locally and inaccuracies are expected in the results yield by the numerical methodology employed. Non-uniformities occur in the vertical direction, but also in horizontal planes (identified by coordinates x and y in this study). Patches of highly-dense flow can occur even at distances from the bottom wall for which sediment concentration is dilute on average. An example of this situation is provided by Fig. 2, where the instantaneous distribution of preferentially-concentrated regions on three wall-parallel monitor planes is shown. Monitor planes are placed in the viscous sublayer at the locations highlighted in Fig. 1, which correspond to the peak of concentration ($z^+ \simeq 2.0$), to the threshold between dilute and semi-dilute flow ($z^+ \simeq 2.9$), and to a reference point inside the viscous sublayer where average concentration is dilute ($z^+ \simeq 4.4$). Based on the values obtained in our simulations and shown in Fig. 1, these regions are labeled as dense (dark gray), semi-dilute (light gray) and dilute (white) if local concentration is $C(x,y,z)/C_{ref} \geqslant 9$, $1 \leqslant C(x,y,z)/C_{ref} < 9$, and $C(x,y,z)/C_{ref} < 1$, respectively. It is apparent that the (x,y)-averaged values of concentration shown in Fig. 1 are determined by spatially-concentrated areas where $C(x,y,z)/C_{ref}$ can grow because of the point-particle 1-way coupling assumption and strong concentration gradients may develop. In the $z^+ \simeq 2.0$ plane, for instance, $C(z)/C_{ref} \simeq 100$ but large areas of dilute flow are visible and dense regions occupy a relatively small proportion of the surface area. This proportion is further reduced on the $z^+ \simeq 2.9$ plane, becoming almost negligible at $z^+ \simeq 4.4$.

To ground the above observations on a quantitative basis, several techniques are available to characterize particle clustering and measure preferential concentration [18]. In this study, we adopt a technique that provides a geometric measure using Voronoi diagrams generated by particle spatial distribution. By construction, a Voronoi diagram is a unique decomposition of an nD space (with $n = 1, 2$ or 3) into independent cells attached to

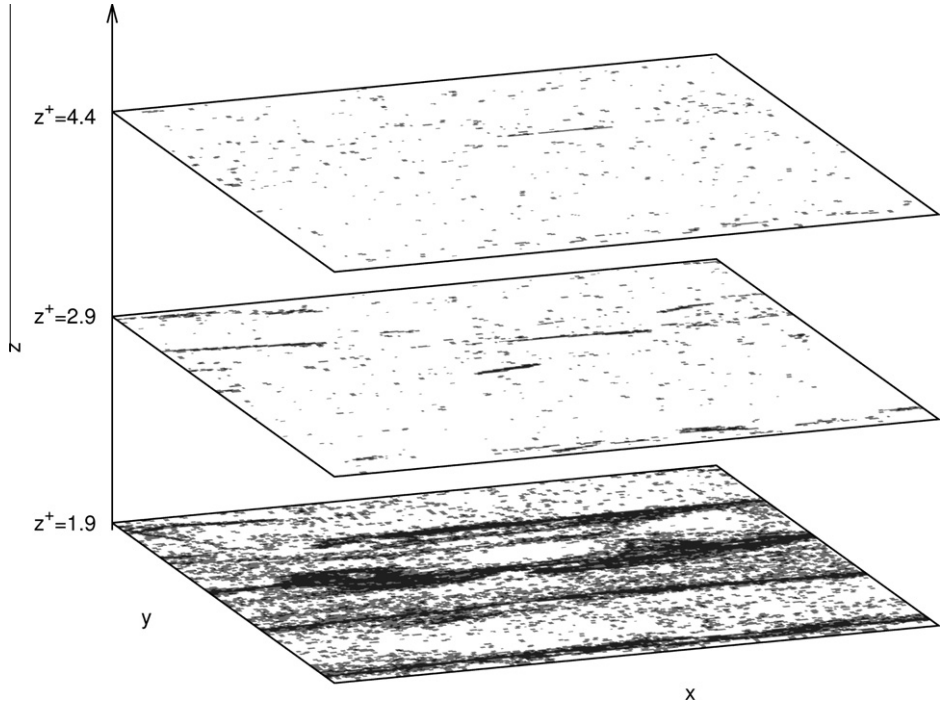

Fig. 2. Instantaneous spatial distribution of dilute (1-way coupled, white), semi-dilute (2-way coupled, light gray) and dense (4-way coupled, dark gray) flow regions near the solid boundary in open channel flow ($St = 0.5,\ Re_\tau = 85.5$). Monitor planes are located at different heights within the viscous sublayer. The simulation time chosen for visualization is the same as for the base-DNS concentration profile in Fig. 1.

individual particles [19]. For a given particle, the corresponding Voronoi cell is given by the ensemble of points that are closer to that particle than to any other: the area (or, in 3D, the volume) of the cell is thus the inverse of the local nD particle concentration. Because of this property, and because it provides grid-independent results, the Voronoi analysis is preferred here to standard box counting techniques [19]. An example of a 2D Voronoi diagram, obtained from the same DNS database used to produce Figs. 1 and 2, is shown in Fig. 3. In Fig. 4, we plot the discrete Probability Distribution Function (PDF) of Voronoi areas generated by tessellation of the three monitor planes shown in Fig. 2 (and expressed in dimensionless values). The vertical solid arrows in each panel indicate thresholds separating the different concentration regions. Probability is evenly distributed over the entire spectrum of areas both in the $z^+ \simeq 4.4$ plane (Fig. 4(a)) and in the $z^+ \simeq 2.9$ plane (Fig. 4(b)). As could be anticipated from analysis of Fig. 2, the PDF exhibits a clear peak (almost equal to unity) when the Voronoi area attains its lowest value in the $z^+ \simeq 1.9$ plane (Fig. 4(c)). Note that a PDF of order $\mathcal{O}(10^{-5})$ corresponds to a single Voronoi cell, namely to a region of the flow almost fully depleted of particles.

Such clustering analyses are becoming routine practice to identify specific topological regions where particles tend to accumulate and can be used to show clearly the limitations which are intrinsic in the Eulerian–Lagrangian (EL) point-particle approach. In this paper we examine critically these limitations, but also the potentials for predicting sedimentation and resuspension phenomena in steady turbulent boundary layer. In particular, we discuss the range of applicability of the point-particle approach to capture vertical fluxes to and off the wall in semi-dilute and/or dense flow conditions. This is done underlining modelling issues associated (i) with the widely diffused method of tracking particles one-way coupled with the fluid but also (ii) with an insufficient resolution of the flow field, typically incurred in LES. To assist discussion, we summarize results from our previous investigations on particle turbulent transfer mechanisms [5,8,20] that are relevant to sediment transport. We focus our attention on the presence of shear which flavors wall turbulence with a unique multi-scale aspect and adds intricacy to the role of inertia and gravity in influencing particle motion [21,22]. We also emphasize the need for a sound rendering of wall turbulence to produce physical understanding of sedimentation and resuspension phenomena [5]. We conclude presenting original DNS-based numerical experiments aimed at reproducing with improved accuracy the flow in the wall region and at assessing potentials of LES as alternative to DNS for higher-Reynolds-number flows.

2. Methodological approach

To analyze sedimentation and resuspension mechanisms, we adopted concepts and modeling ideas derived from a systematic study of the Eulerian turbulent field coupled with LPT under different modeling assumptions [5]. In this paper, we discuss results for three different flow configurations: closed/open plane channel and open wavy channel. In all cases, the governing balance equations are continuity and Navier–Stokes for incompressible fluid, written considering a Eulerian coordinate system with x-, y- and z-axes pointing in the streamwise, spanwise and wall-normal directions, respectively. All variables are made dimensionless using u_τ and the fluid kinematic viscosity $\nu = \mu/\rho$.

Pseudo-spectral DNS was performed for the plane channel configurations (see [5] and references therein for more details). Governing equations are solved using a two-level explicit Adams–Bashforth scheme for the non-linear convection terms and an implicit Crank–Nicolson method for the diffusion terms. All calculations are carried out in the Fourier–Chebychev wave space except for the non-linear terms, which are computed in the physical space and then transformed back to wave space. Periodic boundary conditions are imposed on the fluid velocity field both in x and y, whereas a no-slip (resp. free-slip) boundary condition is imposed at the wall (resp. free surface). Calculations are performed on a computational domain of size $4\pi h \times 2\pi h \times 2h$ in x, y

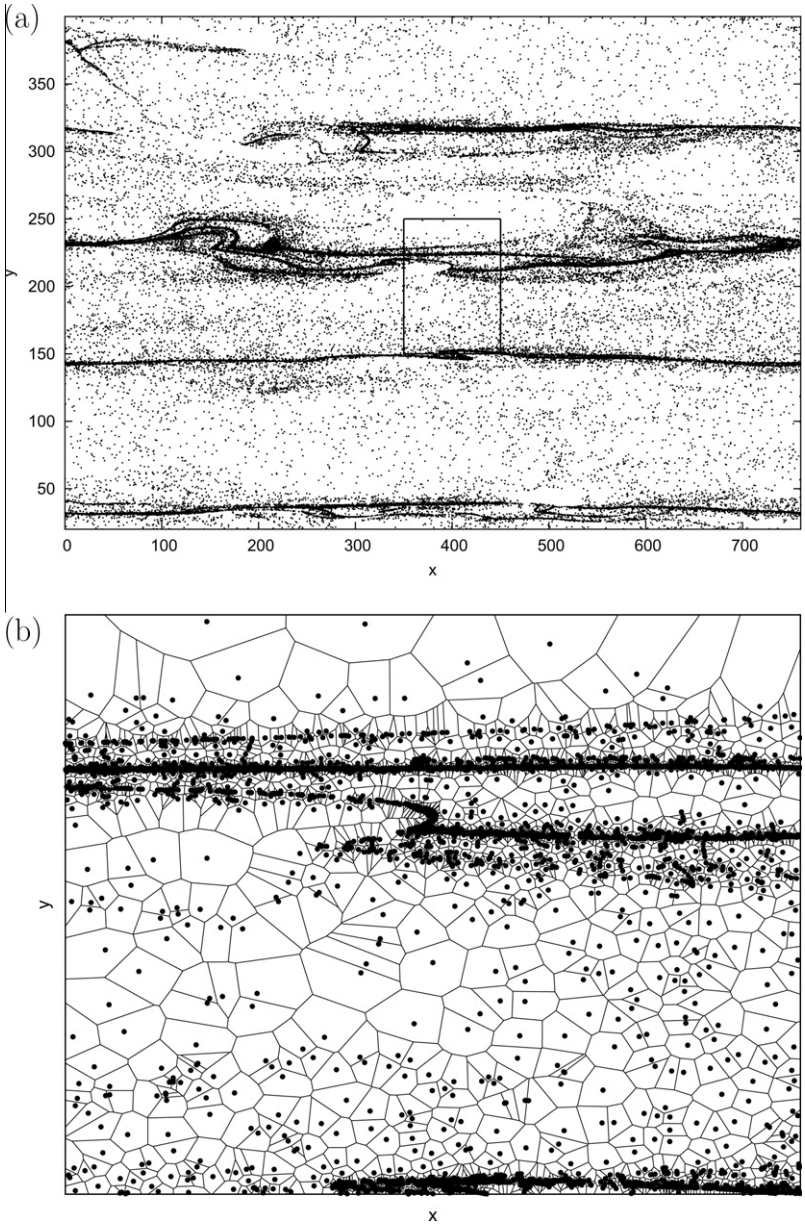

Fig. 3. Instantaneous distribution of $St = 0.5$ sediment particles on the $z^+ = 1.9$ plane shown in Fig. 2 (a) and corresponding Voronoi diagram (b). For clarity, we show the diagram only over a small portion of the full plane.

and z. The shear Reynolds number is $Re_\tau = u_\tau h/\nu$, where h is the channel half height. For closed channel flow, we performed simulations at $Re_\tau = 150$ and 300 with grid resolution $\Delta x^+ = 14.7$, $\Delta y^+ = 7.35$ and Δz^+ ranging from 0.045 to 3.68. For open channel flow, simulations were performed at $Re_\tau = 85.5$ with grid resolution $\Delta x^+ = 8.46$, $\Delta y^+ = 4.23$ and Δz^+ ranging from 0.026 to 2.1.

Note that, to produce results discussed in Section 4.2, DNS datasets were complemented by pseudo-spectral large-eddy simulations (LES) of the same channel flow domain. To this aim, the DNS flow solver was adapted to solve for filtered governing equations closed using the dynamic sub-grid scale (SGS) model of [23].

LES was also performed for the wavy channel configuration (see [8] and references therein for more details). The Navier–Stokes solver uses two sets of variables, defining velocities and pressure at cell centers and contravariant volume fluxes at the cell faces. Equations are transformed into a general curvilinear coordinate system and discretized on a co-located grid using a finite volume approach. The SGS effect on the stress tensor is modeled using the dynamic two-parameter model proposed by [24]. A fractional step method is employed to advance in time, and pressure is obtained by solving a Poisson equation with a multigrid algorithm. Time marching is semi-implicit: the Adams–Bashforth scheme is used for the convective and off-diagonal diffusive terms, whereas the diagonal diffusive terms are treated using the Crank–Nicolson scheme. Overall, the algorithm is 2nd-order accurate in space and time. The reference geometry consists of fixed two-dimensional sinusoidal waves of length λ, with geometry and conditions as in [8]: free-slip stress-free upper boundary, periodic box sides, no-slip lower wavy wall. The domain size is $2\lambda \times \frac{4}{3}\pi H \times H$ in x, y, and z with grid resolution $\Delta x^+ = 7.9$, $\Delta y^+ = 11.0$ and Δz^+ ranging from 1.6 to 7.9. The shear Reynolds number is $Re_\tau = u_\tau H/\nu = 170$, where H is the channel height.

Both DNS and LES flow solvers are coupled to a LPT code that interpolates fluid velocities at discrete grid nodes onto the particle position by means of 6th order Lagrangian polynomials in the

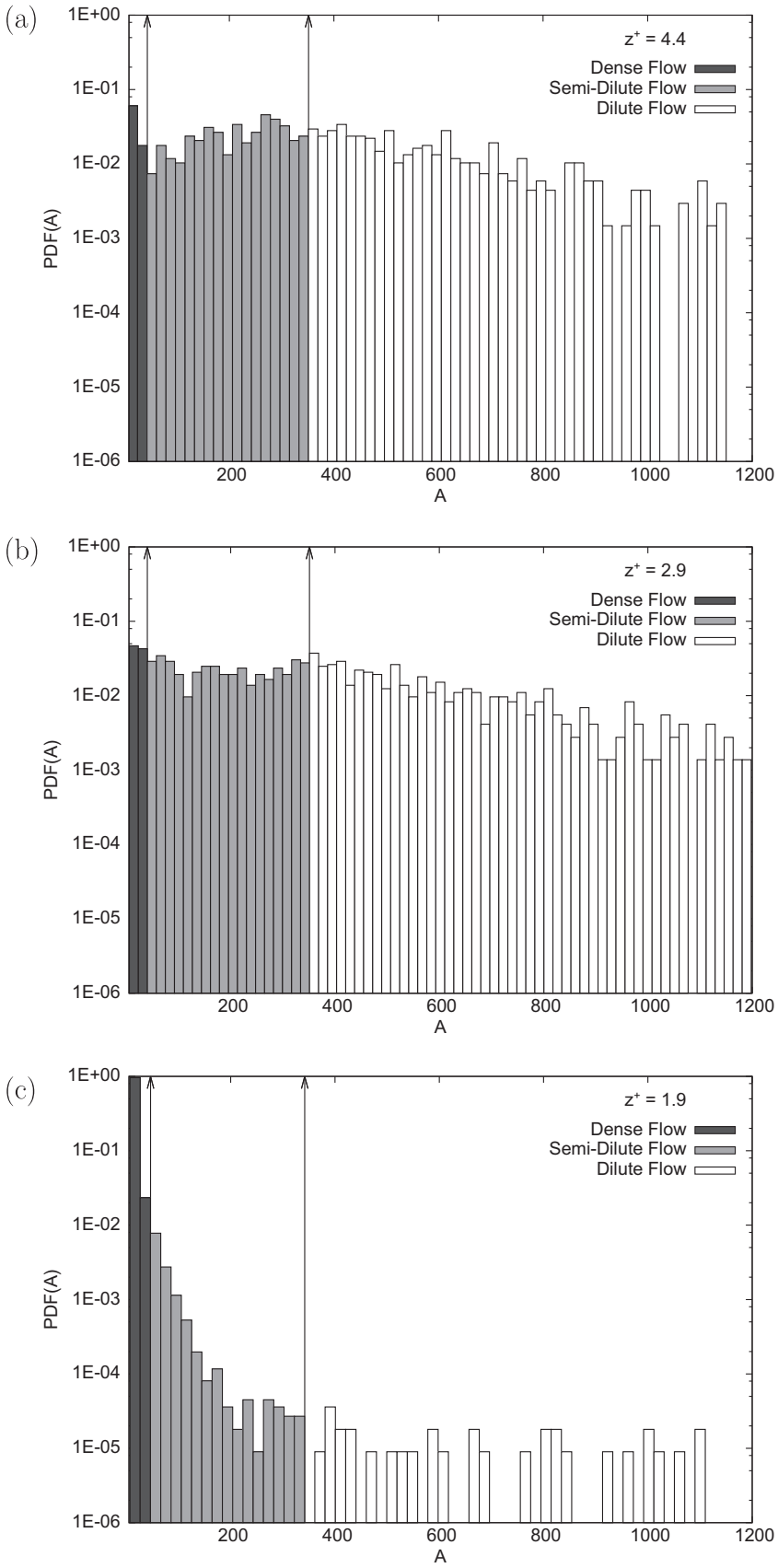

Fig. 4. Discrete PDFs of dimensionless Voronoi areas corresponding to the instantaneous spatial distributions shown in Fig. 2: $z^+ = 4.4$ (a), $z^+ = 2.9$ (b), and $z^+ = 1.9$ (c).

plane channel case and of an *ad hoc* 2nd-order accurate interpolation scheme for the wavy channel case. This scheme is based on the Taylor series expansion of the fluid velocity about the grid point nearest to the particle location and has been developed specifically

for interpolation on curvilinear grids with non-orthogonal computational cells [25]. The equations of particle motion are integrated in time using a 4th order Runge–Kutta scheme in DNS fields and an explicit 2nd-order modified Euler method in LES fields. Particles are non-interacting, pointwise, rigid, spheres initially released at random locations within the computational box. A particle is elastically reflected away from the wall when its center is less than one particle radius from the wall. Because of the particle-to-fluid density ratio, particle momentum balance equation is simplified neglecting virtual mass, pressure gradient force and Basset force. The only forces considered in closed channel simulations were inertia and drag. Gravity was also included in the open channel simulations (parameterized by the Froude number, $Fr = \langle u_{rms} \rangle / \tau_p g$, u_{rms} being the root mean square of the fluid velocity fluctuations) whereas lift was included in the wavy channel simulations. To evaluate the effect of particle inertia, several sets of particles characterized by different values of the Stokes number, accounting for differences in particle size and/or specific density, were tracked in each flow configuration: specifically, we considered $0.2 < St < 125$ in closed channel flow (corresponding to particles with diameter ranging from 25 to 280 μm and specific density $\rho_p/\rho_f \simeq 2$ in a 1-cm high water channel) [5], $0.05 < St < 0.5$ in open channel flow (corresponding to particles with diameter ranging from 50 to 150 μm and specific density $\rho_p/\rho_f \simeq 2$ in a 1.2-cm high water channel) [10], and $0.1 < St < 2$ in wavy channel flow (corresponding to particles with diameter ranging from 35 to 160 μm and specific density $\rho_p/\rho_f \simeq 2$ in a 2-cm high water channel) [8]. We remark that dimensional values for fluid and particle parameters were selected to ensure fully-turbulent flow conditions and fully-respected assumptions (e.g. pointwise particles), albeit in a marginal range for large-scale applications: the strategy behind this choice is to verify the physics (which should scale) through DNS and export knowledge to more realistic LES.

3. Phenomenology of particle sedimentation and resuspension in turbulent boundary layers

To frame the applicability of the EL point-particle approach to sedimentation and resuspension problems, we first provide a general overview of particles–turbulence interactions in boundary layers. Findings presented in this section were obtained from previous studies of particle transfer mechanisms in turbulent two-phase flows [5].

3.1. Sedimentation and resuspension over smooth flat surfaces

A pictorial view of particle transfer mechanisms over flat surfaces is provided in Fig. 5. This figure refers to a DNS-based simulation of $St = 25$ particles in turbulent channel flow at $Re_\tau = 150$ [5] and focuses on an area of strong particle accumulation between neighboring vortices in the near-wall region of the channel. Fig. 5(a) shows the instantaneous distribution of the particles (circles) superposed to the local flow field, with vectors representing the in-plane fluid velocity and colored iso-contours mapping the values of the streamwise fluid velocity. To emphasize the correlation between particle dynamics and near-wall turbulence dynamics, we discriminate between particles with wall-normal velocity directed away from the wall (red[1] circles), particles with wall-normal velocity directed toward the wall (gray circles) and particles with negligible wall-normal velocity (blue circles). Strongly coherent ejections of low-momentum fluid and in-sweeps of high-momentum fluid are evident in the central part of the figure, where two low-speed streaks (LLSS), lifted and flanked by counter-rotating vortices (QSV), can be observed. In Fig. 5(b) we show the same flow field but this time we illustrate the transport mechanisms that determined by the physics depicted in Fig. 5(a). First, particles segregate and form coherent clusters in regions of the buffer layer where in-sweeps can entrain them: segregation into clusters is thus the first mechanism characterizing the sedimentation process. Particles entrained in a sweep experience a net drift toward the near-wall accumulation region, where particle concentration reaches its maximum (see Fig. 1). When considering inertial sediment particles, such drift is mainly driven by turbophoresis (see [20] and references therein). Once in the accumulation region, which is located well into the viscous sublayer, particles may either deposit at the wall or be re-entrained toward the outer flow by ejections. Two main sedimentation mechanisms can be identified: particles that have acquired enough momentum may coast through the accumulation region and deposit by impaction directly at the wall; otherwise particles can slowly deposit under the action of residual near-wall turbulent fluctuations that, due to turbulence non homogeneity, are always stronger in driving particles to the wall. The relative importance of these mechanisms depends on particle inertia. The main re-entrainment mechanisms are also two: particles may be either resuspended immediately by the same vortex which brought them to the wall or confined for very long times in the viscous region. As a consequence, particle transfer fluxes toward the wall have higher intensity than particle transfer fluxes away from the wall. In turn, unbalanced fluxes lead to nonuniform (preferential) distribution of particles within the flow and produce near-wall accumulation (see [20] and references therein). The phenomenological picture drawn from Fig. 5 applies fully to heavy inertial particles [5,20], but also to lighter sediment particles as also demonstrated by dedicated experimental [12,26–29] and numerical [4,30] studies. In the next section, we show how it can be extended to more complex wall geometries (rough walls in particular).

3.2. Sedimentation and resuspension over wavy interfaces

Open channels with wavy bottom wall are customarily used to study sediment transport over ripples or rough bed-forms via numerical simulations [4,7,8]. A snapshot of sediment distribution in the proximity of wavy ripples is provided in Fig. 6, which refers to the solid–liquid turbulent flow in horizontal channel reported in [8]. In this figure, particles have $St = 0.1$ (light sediments) and are shown together with the near-wall vortical structures, visualized as isosurfaces of the streamline rotation vector [31]. Particles transfer to and off the wall due to vortices is apparent: a vortex can be found at or near the preferential locations where particles penetrate and exit the wall layer. This interaction is selectively modulated by sediment inertia and can be parameterized by the Stokes number. As particle inertia increases, particle behavior decouples from the dynamics of the turbulence structures, hence decreasing the extent of the interaction [8]. Sweep and ejection events are also important [29]. Sweeps represent descending flow close to the downwash sides of the vortices and produce higher-than-mean shear stress regions at the wall (dark gray areas in Fig. 6). Ejections represent ascending flow found in between the vortices and generate lower-than-mean shear stress regions at the wall (light gray areas in Fig. 6). In Fig. 7, we correlate the instantaneous position of sediment particles with the location of sweeps and ejections at varying particle inertia. Focusing on the lighter particles [$St = 0.1$, Fig. 7(a)], there is evidence of a strong correlation between wallward-moving particles (black dots) and sweeps (dark gray iso-contours), since only a small fraction of the particles falls out of sweep regions. In turn, the position of the particles moving away from the wall (gray dots) correlates well

[1] For interpretation of color in Fig. 5, the reader is referred to the web version of this article.

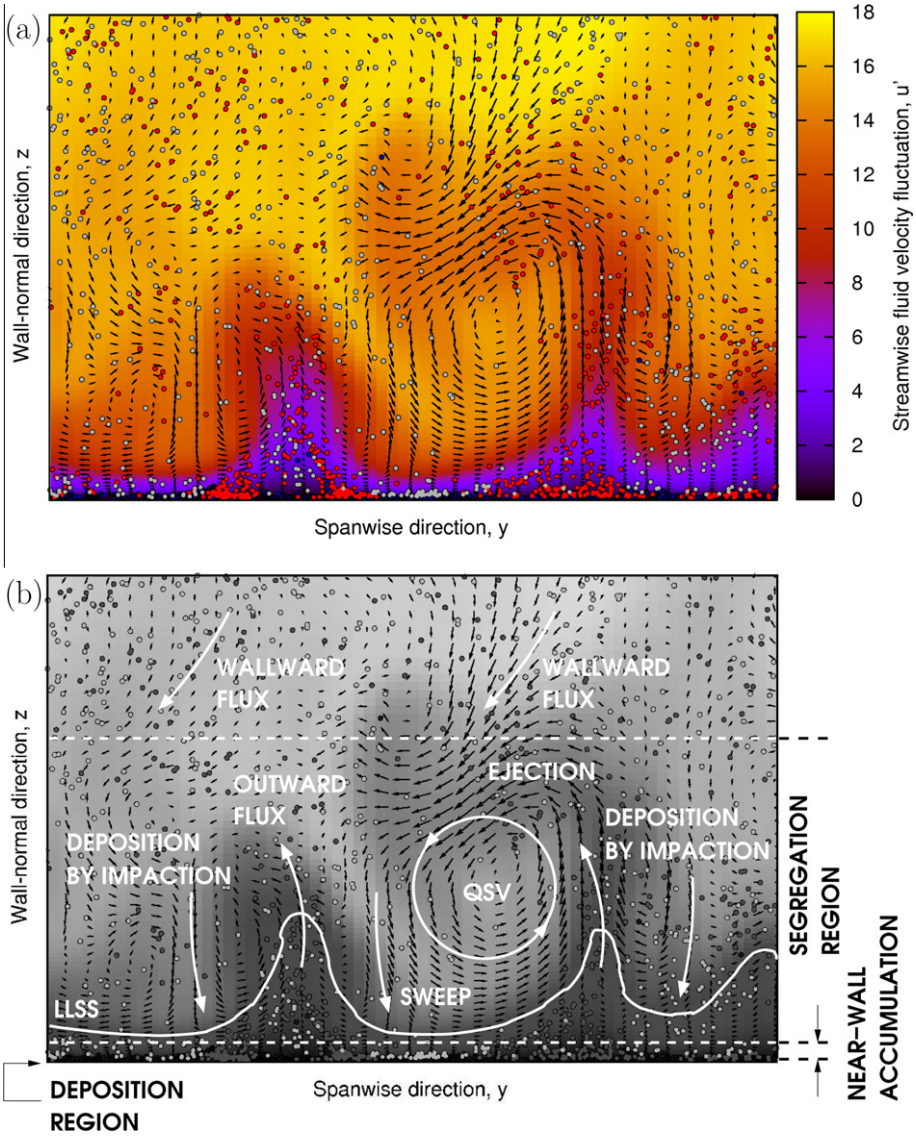

Fig. 5. Instantaneous flow field and sediment distribution in near-wall regions of strong accumulation (a); illustration of turbulent transport mechanisms driving concentration build-up in the deposition region (b).

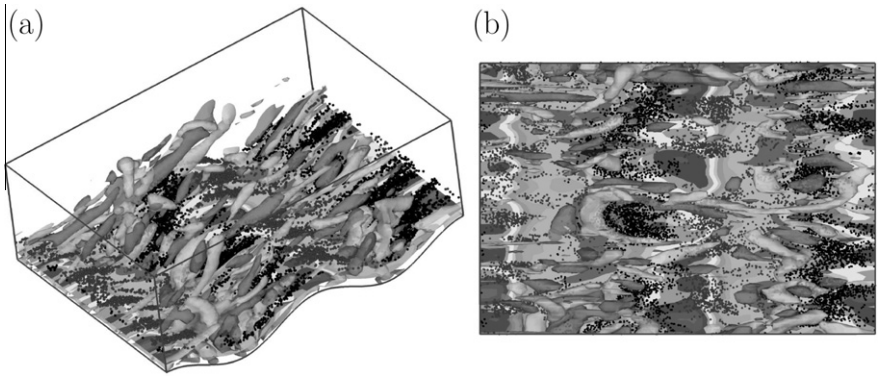

Fig. 6. Perspective view (a) and top-down view (b) of sediment particle and coherent vortical structures over a wavy interface. Dark gray (resp. light gray) Ω-isosurfaces indicate clockwise-rotating (resp. counterclockwise-rotating) vortices. Black (resp. gray) particles have negative (resp. positive) vertical velocity and move downward (resp. upward). For visualization purposes, only those particles crossing a sinusoidal surface at a distance $Z^+ = 15$ from the bottom wall are shown.

with the instantaneous position of ejections (light gray contours). The area of the wave over which particle resuspension occurs most actively seems to be the wave upslope, characterized by large wall-shear stress and high turbulent fluctuations; sedimentation occurs most actively in the wave downslope and the trough, where small wall-shear stress and low turbulent fluctuations are found [7,8].

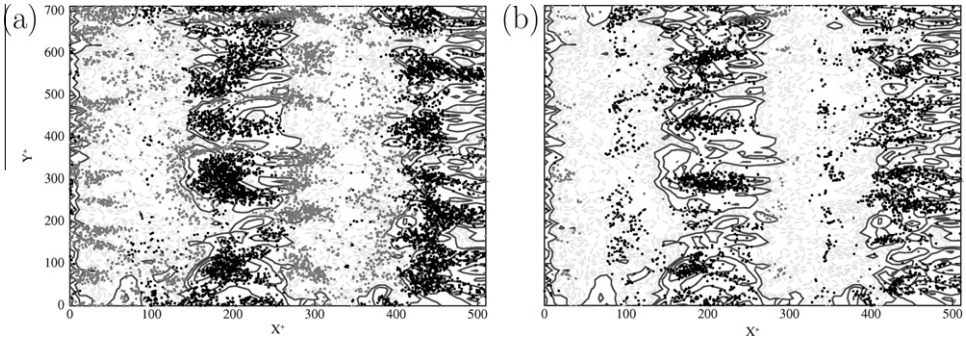

Fig. 7. Inertial effects on the correlation between wall-shear stress distribution, sedimentation fluxes (gray dots) and resuspension fluxes (black dots): (a) light $St = 0.1$ particles, (b) heavy $St = 2.0$ particles. Snapshots are taken at the same time of Fig. 6. Dark gray (resp. light gray) contours represent locations where shear is higher (resp. lower) than its mean value $\bar{\tau}$ on a monitor surface at $Z^+ = 15$ from the wavy wall.

This picture holds for the heavier particles [$St = 2.0$, Fig. 7(b)], even if spatial correlations weaken due to increased inertia and very little resuspension is observed. The transfer mechanisms just highlighted are similar to those controlling heavy particles dispersion in gas–solid flows in plane channels [5,20]. Hence the same phenomenological frame-model for particle transfer and dispersion in turbulent boundary layer can be applied. This model is presented in the next section, where its predictive capabilities and modelling limitations in the context of sediment dispersion problems are discussed.

4. Assessing modelling issues in Eulerian–Lagrangian simulations of sediment dynamics

Current modelling issues in EL simulations of turbulent sediment dynamics are mainly due to three factors which complicate the physical problem: flow geometry, flow Reynolds number and near-bed density of the flow. When complex flow geometries and high Reynolds numbers have to be dealt with, LPT in flow fields obtained from LES may represent a potentially useful tool for the analysis of sediment-laden flows and for the prediction of vertical mixing in turbulent boundary layers. Applicability of LES to such flows, however, is still limited and further efforts are required to improve quality and reliability of LPT in LES flow fields. Additional complexity is added when high sediment density exists near the boundary (e.g. induced by sheet flow), which requires accurate modelling of sediment interactions with the boundary (treated as a solid wall from a computational viewpoint). In the following we highlight the most relevant issues related to the numerical treatment of particle–wall interactions and to the use of LPT in LES flow fields.

4.1. Modelling particle–wall interactions with the point-particle approach

The most accurate numerical technique currently available to simulate sediment dynamics in turbulent flow is the so-called fully-resolved turbulence [13]. This technique, which solves for all the turbulent scales of the flow around the sediment particle, is very expensive from a computational viewpoint and does not allow simulation of large swarms of particles – $\mathcal{O}(10^4)$ or more – with present-day computers. An alternative, computationally faster technique is the point-particle approach, in which the fluid velocity interpolated at the center of the particle is all one needs to calculate the forces acting on individual particles when these are significantly smaller than the smallest turbulence scales. Even though point-particle simulations are well known [1], it is not clear to what extent the treatment of particle–wall interactions can affect the accuracy of the simulations when applied to sedimentation problems. In particular, the length scale (distance from the bottom wall) at which local effects in particle concentration make the 1-way coupling assumption unacceptable is yet to be determined. To discuss these issues, we focus on one relevant observable: the vertical mixing of suspended sediments in open channel flow, already discussed in Fig. 1. If no particle–particle interaction (e.g. collisions) is accounted for in the numerics then areas densely populated by sediments form very near the wall where the local volume fraction can grow unbounded. It is thus expected that simulations based on 1-way coupling provide an over-estimation of particle accumulation at the wall. This behavior changes dramatically when particles are prevented from sampling regions of the flow already occupied by the maximum number of particles per unit volume (*saturated volume*): particle concentration cannot reach unphysically-high peaks (allowed by the point-particle approach and by the 1-way coupling assumption) anymore. In Fig. 8, we quantify this change when a simple model accounting for saturated volume effects is implemented: given the rebound position of a target particle, $P(x_{reb}(t), y_{reb}(t), z_{reb} = d_p/2)$, computed from the base simulation, this model mimics the presence of a near-bottom sediment layer with finite thickness by adapting the vertical height of rebound as $\tilde{z}_{reb} = z_{reb} + z_s$. The shift z_s depends on the number of particles n_p found inside the boundary cell of size $\Delta x \times \Delta y \times \delta z$ (with δz chosen arbitrarily) within which the target particle rebounds: $z_s = n_p V_p / \Delta x \Delta y$, with V_p the particle volume, and hence $V_{sat} = \Delta x \Delta y z_s$ the saturated volume. Fig. 8, taken at the same time instant of Fig. 1, shows clearly that the agreement between the numerical result and the Rouse prediction decreases since it is maintained only in the outer flow region ($z^+ > 30$) and that modifications of the rebound height have a dramatic effect on the relative intensity of sedimentation and resuspension fluxes. The net downward flux decreases by nearly one order of magnitude with respect to the case in which particle rebound occurs at z_{reb} and no high-density flow region (where collisions must be accounted for) has developed yet. In fact, the concentration peak has shifted away from the bottom boundary (its value being closer to that of experiments [27]) and only regions of semi-dilute flow with significant two-way coupling effects are observed.

Another modelling issue associated to particle–wall interaction is related to particles collision with rough walls rather than smooth walls. The presence of a small-scale wall roughness can alter significantly sediment dynamics, and vertical mixing of suspended sediments in particular, even when the flow dynamics are not affected [32]. Roughness effects on vertical mixing in turbulent boundary layer are shown in Fig. 9 for the case of $St = 100$ particles in closed channel flow at $Re_\tau = 150$. Wall roughness is reproduced here adopting the Multi-Wall Collision Model (MWCM) proposed by Konan et al. [32], in which the wall roughness angle γ is chosen with

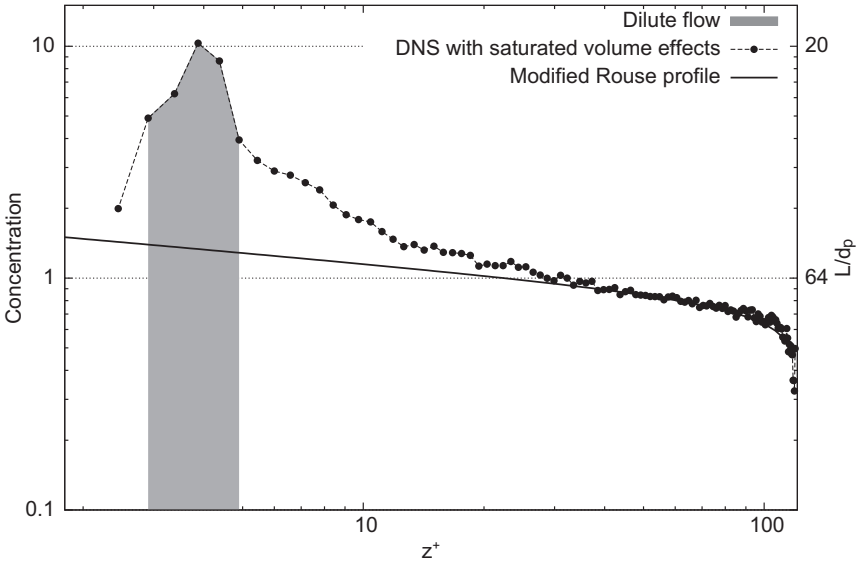

Fig. 8. Vertical mixing of sediment particles in turbulent boundary layer: comparison of concentration profiles from point-particle DNS (symbols) with saturated volume effects against modified Rouse model prediction (solid line). Particle rebound is modified to account for local dense flow effects and occurs at $\bar{z}_{reb} = d_p/2 + z_s$.

respect to a probabilistic distribution law that is uniform, Gaussian with zero mean and standard deviation $\Delta\gamma$. Fig. 9(a) clearly shows that roughness acts as a *disordering agent* that enhances vertical mixing [33] by redistributing particles within the flow and reduces near-wall accumulation. This reduction results from a modification of transport fluxes to and off the wall, as shown in Fig. 9(b) and (c): compared to the case of smooth walls [Fig. 9(b)], roughness acts to balance sedimentation fluxes (N_{sed}, solid line) and resuspension fluxes (N_{res}, dotted line) [Fig. 9(c)]. Fig. 9(a) provides a rough indication of the degree of particle redistribution produced by roughness and highlights the extent of the length scale over which roughness effects can not be neglected. Results shown in this figure suggest that roughness effects on vertical mixing in dilute flow are similar to those produced by saturated volume effects in dense flow, and thus both elementary processes should be taken into account in high-fidelity simulations [36]. In sedimentation problems, in particular, this is crucial to reproduce particle resuspension processes when adopting the point-particle approach with one-way coupling only. In real situations, resuspension is promoted by the high particle concentration gradients that form near the bottom wall, but also by an increase of particle–particle interaction rates. Compared with these effects, resuspension due to a skewed distribution of the fluid velocity fluctuations in the vertical direction is much less significant [27].

Even if particle–wall and particle–particle interactions are treated with the most accurate models currently available (e.g. MWCM [32] and hard-sphere models [34,35] for EL computations), problems still arise when the resolution of the flow field is insufficient. This is precisely the case of LES, where only an approximation of the exact flow field is available. In the next section, we will examine limitations of LPT in LES fields associated with the use of an approximate fluid velocity. In particular, we will show that, different from single-phase flows, in which the amount of energy filtered is the significant variable to model, in current cases this is not enough to warrant correct statistical characterization of particle motion. We will also discuss possible strategies to overcome such limitations in the EL framework.

4.2. Quality and reliability of LPT in LES flow fields

Current applicability of LES to particle-laden flows is limited mainly by the modeling of the SGS turbulence effects on particle dynamics [37,38]. As a result, LES fails to predict quantitatively sedimentation and resuspension fluxes in environmental flows. Attempts have been made to improve predictive capabilities of LES by accounting explicitly for SGS effects through *ad hoc* closure models in the Lagrangian equation of particle motion [37–39]. These attempts, however, show that even if the fraction of SGS turbulent kinetic energy for the fluid velocity field (not resolved in LES) is recovered, quantitative prediction of local segregation and, in turn, of near-wall accumulation may still be inaccurate [37].

An example of the effect produced on vertical mixing by LPT in LES flow fields with and without particle closure models is shown in Fig. 10, where the instantaneous concentration profiles of sediments with different inertia (different Stokes number) dispersed in turbulent closed channel flow at $Re_\tau = 150$ is reported. In all cases, near-wall concentration is underestimated with respect to DNS, which is regarded as the exact reference in the context of the present analysis. We recall that, for comparison purposes, LES and DNS in the plane channel configuration were both performed using a pseudo-spectral code. The inclusion of a closure model for the particles (based on sequential approximate deconvolution [40] and fractal interpolation [41] of the filtered fluid velocity field obtained from LES, in Fig. 10) improves the agreement with DNS [38,39] yet does not remove discrepancies even when LES fields are well-resolved. In the specific case of approximate deconvolution, this result can be explained considering that the inverse filtering operation intrinsic of such technique only acts on the resolved fluid scales. Given the LES flow field $\overline{\mathbf{u}}$, the deconvolved velocity field, $\mathbf{u}^*$, can be obtained as:

$$\mathbf{u}^* = \sum_{\alpha=0}^{N} (1 - G)^{\alpha} * \overline{\mathbf{u}} = G^{-1} * \overline{\mathbf{u}}, \tag{2}$$

where G is a filter kernel (e.g. top-hat filter), G^{-1} its inverse, and N is the series truncation parameter, usually set equal to 5 [40]. In the best case scenario, this velocity field may regain the energy subtracted from the resolved scales by filtering, but not the energy associated with the non-resolved subgrid scales.

This subgrid energy can in principle be recovered by fractal interpolation: this technique reconstructs the filtered scales using an affine mapping procedure to *extrapolate* the coarse-grained LES field to smaller and smaller scales [41]. In the case of Fig. 10, a 1D

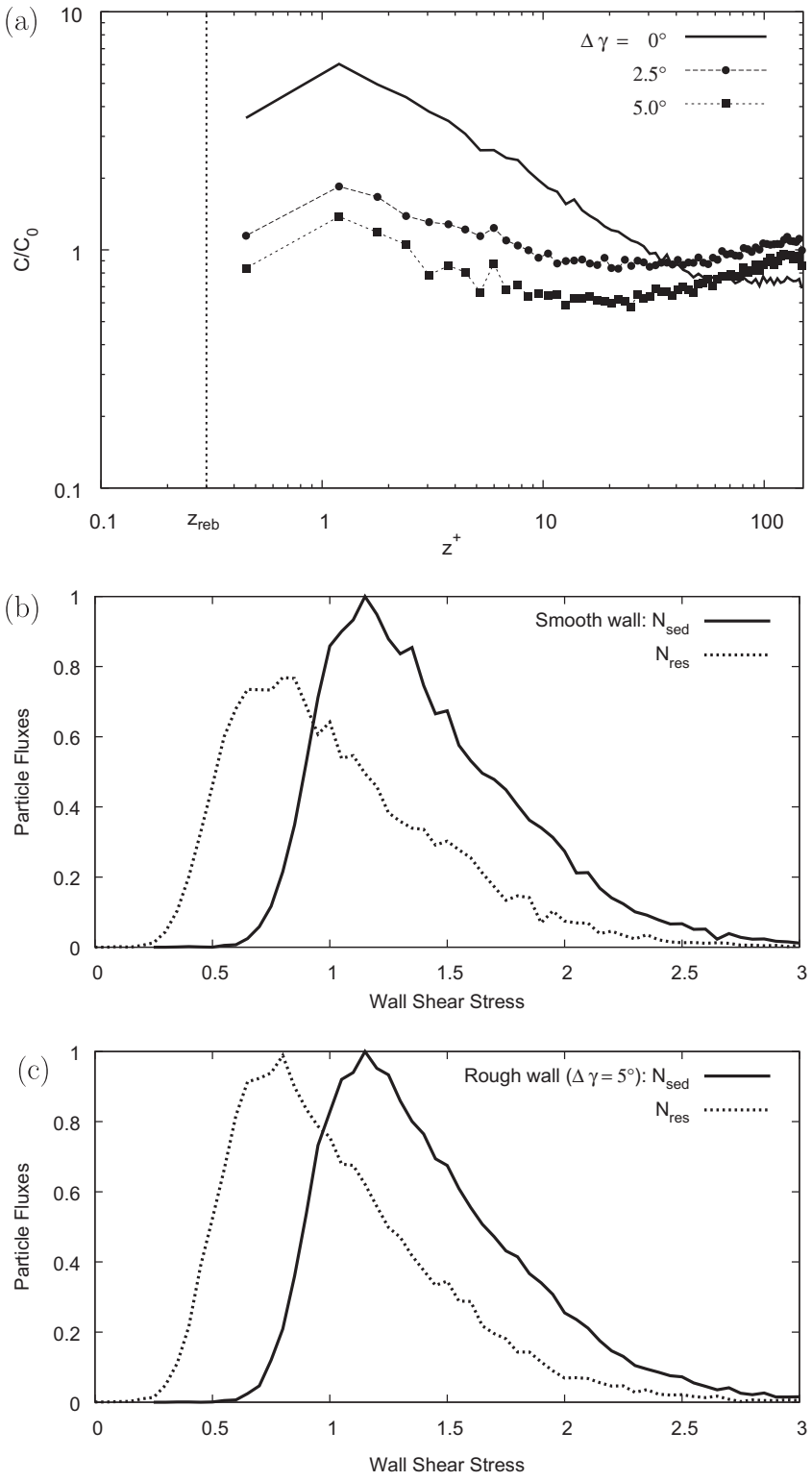

Fig. 9. Vertical mixing of sediment particles in turbulent boundary layer: comparison of numerical concentration profiles (a) and mass fluxes (b–c) from point-particle DNS with and without wall roughness.

mapping procedure was applied iteratively to the deconvolved velocity $\mathbf{u}^*$ in each homogeneous direction, starting from the coarse LES grid on which $\mathbf{u}^*$ is available and ending on the fine DNS grid. The fractally-interpolated flow field is thus obtained as:

$$W_i[u](\xi) = d_1 \cdot u^*(2\cdot\xi) + q_{i,1}(2\cdot\xi) \quad \text{if } \xi \epsilon \left[0, \frac{1}{2}\right], \tag{3}$$

$$W_i[u](\xi) = d_2 \cdot u^*(2\cdot\xi - 1) + q_{i,2}(2\cdot\xi - 1) \quad \text{if } \xi \epsilon \left[\frac{1}{2}, 1\right], \tag{4}$$

where $\xi = (x - x_{i-1})/2\Delta$ is a dimensionless coordinate in the interval $[x_{i-1}, x_{i+1}]$, $x_{i-1} < x < x_{i+1}$ and:

$$q_{i,1}(\xi) = [u_i^* - u_{i-1}^* - d_1 \cdot (u_{i+1}^* - u_{i-1}^*)] \cdot \xi + u_{i-1}^* \cdot (1 - d_1), \tag{5}$$

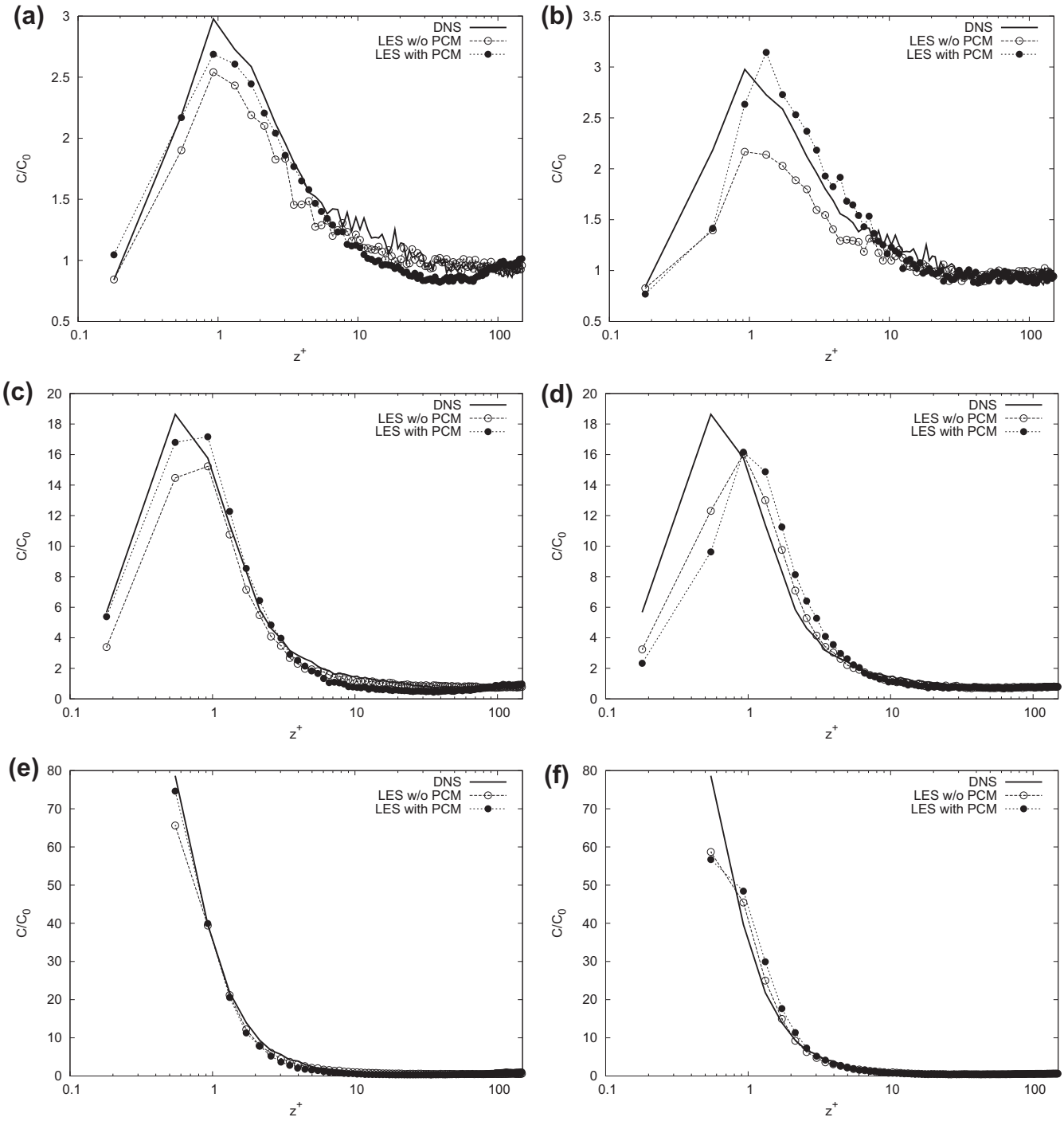

Fig. 10. Effect of particle closure model on concentration: comparison between DNS (solid line), LES (open circles) and LES with Particle Closure Model (PCM) based on approximate deconvolution coupled with fractal interpolation (black circles). Panels: (a) and (b) $St = 1$; (c) and (d) $St = 5$; (e) and (f) $St = 25$. Left-hand panels are relative to a well-resolved LES; right-hand panels are relative to a coarse-grained LES [37].

$$q_{i,2}(\xi) = [u^*_{i+1} - u^*_i - d_2 \cdot (u^*_{i+1} - u^*_{i-1})] \cdot \xi + u^*_i - d_2 \cdot u^*_{i-1}, \qquad (6)$$

with d_1 and d_2 the stretching parameters given by the fractal dimension of the velocity signal [37,41]. Because of the flow anisotropy, these parameters were computed locally, without the a priori knowledge of the fractal dimension of the velocity signal, and subsequently stored in look-up tables (the reader is referred to [37] for a detailed description of the procedure followed to obtain d_1 and d_2).

Results of Fig. 10 indicate that the combination of the two techniques is not enough to reproduce the effect of SGS turbulence on particles and recover the DNS prediction. This failure suggests that, besides reconstructing the correct amount of fluid and particle velocity fluctuations, further information on the flow structure at the sub-grid scales must be incorporated. The same behavior has been observed for a significant range of Reynolds number in the low to intermediate regime [37]. A physical explanation to it is provided in Fig. 11, where a cross-sectional view of particles and vortical structures as captured by DNS (top panel) and by LES (bottom panel) is shown. Particles are drawn as light-gray circles, larger than the real scale for visualization purposes. Vortical structures are rendered using streamwise vorticity isosurfaces: the gray iso-

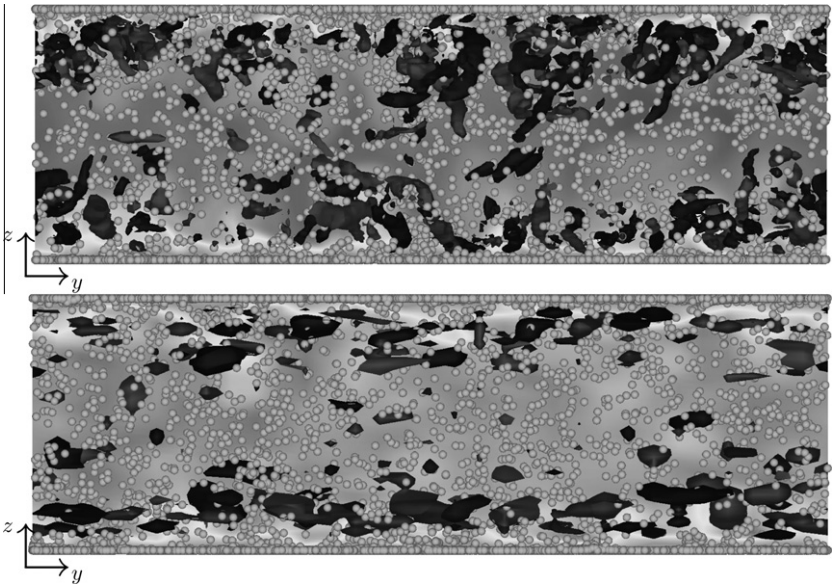

Fig. 11. Front view of particle instantaneous distribution and turbulent structures in closed channel flow: DNS (top) versus LES (bottom). Vorticity iso-surfaces are drawn selecting values equal to ±15% of the instantaneous maximum/minimum of vorticity to capture only the strong vortices.

surface identifies a clockwise rotating quasi-streamwise vortex, whereas the dark gray isosurface identifies a counter-clockwise rotating quasi-streamwise vortex. The graymap in background provides a qualitative visualization of the streamwise fluid velocity distribution in the cross plane: dark tones represent maximum velocity ($u_x^+ \simeq 17$), light tones represent minimum velocity ($u_x^+ \simeq 0$). Differences in the vortical structures between DNS and LES are quite evident, both near the wall and in the center of the channel: sub-grid scales are filtered in LES and, therefore, vortical structures are not properly captured (when not fully ignored) at the finest flow scales. As a consequence, modifications in particles interaction with these structures are expected: indeed, Fig. 11 shows that particles in LES exhibit a more persistent stability against non-homogeneous distribution and near-wall concentration, suggesting less efficient interactions between the two phases and weaker turbophoretic effects.

A promising way to reduce quantitative discrepancies between LES and DNS seems to be represented by the development of a generalized stochastic Lagrangian model for the fluid velocity seen by the sediment particles along their trajectory (referred to velocity *seen* hereinafter). Errors in the velocity *seen* are due to filtering, an intrinsic operation of the LES formalism that can not be avoided. In bounded flows, these errors are non deterministic and exhibit a marked non-Gaussian statistical distribution [42]. Hence, the most natural framework to develop a stochastic SGS model for the particle phase is the probability density function approach. With this approach the fluid velocity *seen* can be modeled using a modified Langevin equation in which the standard drift and diffusion terms are accompanied by an additional term representing a Poisson-like process. This purely-Lagrangian term is included to reproduce the effect of the turbulent structures (sweeps, ejections, quasi-streamwise vortices – see Section 3) that control sediment dynamics in the near-wall region. The hope is to correct filtering errors and to recover the levels of preferential concentration and wall-accumulation predicted by DNS. Given the intermittent nature of turbulent structures, however, a thorough characterization of their statistical signature (e.g. frequency of occurrence, intensity, geometrical features) is crucial to construct the stochastic process. In spite of recent efforts in this direction [42], much more work remains to be done. In particular, statistical investigation of the Lagrangian properties of the SGS velocity *seen* is required. In our opinion, this can only be achieved computing statistical moments conditioned on specific subsets of particles sampling prescribed topological regions of the flow [42].

5. Conclusions

Starting from current understanding (also developed in our group) of particle dispersion in turbulent boundary layer, in this paper we examine possible modelling strategies to simulate sedimentation and resuspension in high-Reynolds-number flows. These strategies are proposed to overcome current limitations associated with the use of particle tracking methods based on the assumption of one-way coupling between fluid and particles and with an insufficient resolution of the flow field. We evaluate numerically critical conditions where locally-high concentration values may forbid assuming very dilute flow, and intermittencies in particle concentration may not be represented by a single volume-averaged indicator. We also try to circumvent demanding accurate reproduction of the real physics by mimicking near-bottom dense flow regions with ad hoc boundary conditions. To these aims, we use datasets obtained from numerical simulations based on the EL point-particle approach. We examine well-known instances of boundary layer flow in closed/open channels to discuss how this approach can be exploited to analyze the effect of near-wall turbulent coherent structures on sediment deposition and re-entrainment. Our results show that, even in the limit of one-way coupling between particles and fluid, LPT in DNS fields can provide accurate estimate of transfer fluxes in those regions of the flow where turbulent structures determine particle preferential organization in segregated patterns. This methodology becomes inadequate in dense flow regions where realistic modelling of particle–wall interactions (e.g through incorporation of saturated volume effects or roughness effects) and of particle–particle interactions (through collisions kernels) becomes essential to quantify deposition and resuspension fluxes. In the specific context of sedimentation, these findings must be evaluated considering that the Reynolds number of "real-life" sediment suspension flows is typically high and computationally too expensive for DNS. This makes LES a straightforward alternative for numerical investigations [7,8]. Results presented in this paper, however, dem-

onstrate that current capabilities of LES in predicting dispersed flows are strongly limited by the modelling of the sub-grid scale turbulence effects on particle dynamics, and indicate that further efforts must be taken in this direction. One possible solution might be represented by the inclusion of wall layer models [43,44], which are currently used to predict flow separation in aeronautical applications, or heat/mass transfer rates in industrial applications.

Acknowledgments

COST Action MP0806 is gratefully acknowledged. CINECA (Bologna, Italy) is also gratefully acknowledged for having provided computational resources. Finally, the authors would like to thank Salvatore Lovecchio and Ilario de Fort for performing some of the simulations.

References

[1] Special issue on point-particle model for disperse turbulent flows. In: Elghobashi S, editor. Int J Multiphase Flow 2009;35:791–878.
[2] Floris R, van Thienen P. Experimental investigation of turbulent particle radial transport processes in DWDS using optical tomography. Drink Water Eng Sci 2011;4:61–83.
[3] Swamee PK. Design of sediment-transporting pipeline. J Hydraul Eng – ASCE 1995;121:72–6.
[4] Chang YS, Scotti A. Entrainment and suspension of sediments into a turbulent flow over ripples. J Turbul 2003;4:1–19.
[5] Soldati A, Marchioli C. Physics and modelling of turbulent particle deposition and entrainment: review of a systematic study. Int J Multiphase Flow 2003;35:827–39.
[6] Soldati A. Particles turbulence interactions in boundary layers. Z Angew Math Mech 2005;85:683–99.
[7] Widera P, Ghorbaniasl G, Lacor C. Study of the sediment transport over flat and wavy bottom using large-eddy simulation. J Turbul 2009;10:1–20.
[8] Marchioli C, Armenio A, Salvetti MV, Soldati A. Mechanisms for deposition and resuspension of heavy particles in turbulent flow over wavy interfaces. Phys Fluids 2006;18:025102.
[9] Toorman EA. Vertical mixing in the fully developed turbulent boundary layer of sediment-laden open channel flow. J Hydraul Eng – ASCE 2008;134:1225–35.
[10] Lovecchio S. Direct numerical simulation of particle sedimentation and resuspension mechanisms in turbulent boundary layer. MS thesis, University of Udine; 2011.
[11] Rouse H. Modern conceptions of the mechanics of turbulence. Trans Am Soc Civ Eng 1937;102:435–505.
[12] Kiger KT, Pan C. Suspension and turbulence modification effects of solid particulates on a horizontal turbulent channel flow. J Turbul 2002;3:1–21.
[13] Chan-Braun C, Garcia-Villalba M, Uhlmann M. Direct numerical simulation of sediment transport in turbulent open channel flow. In: Nagel WE et al., editors. High performance computing in science and engineering. Berlin Heidelberg: Springer-Verlag; 2011.
[14] Marchioli C, Soldati A, Kuerten JGM, Arcen B, Tanière A, Goldensoph G, Squires KD, Cargnelutti MF, Portela LM. Statistics of particle dispersion in direct numerical simulations of wall-bounded turbulence: results of an international collaborative benchmark test. Int J Multiphase Flow 2008;34:879–93.
[15] Ozdemir CE, Hsu TJ, Balachandar S. A numerical simulation of lutocline dynamics and saturation of fine sediment in the oscillatory boundary layer. J Geophys Res – Oceans 2011;116:C09012.
[16] Ozdemir CE, Hsu TJ, Balachandar SA. numerical investigation of fine particle laden flow in oscillatory channel: the role of particle-induced density stratification. J Fluid Mech 2010;665:1–45.
[17] Hsu TJ, Jenkins JT, Liu PLF. On two-phase sediment transport: sheet flow of massive particles. Proc Roy Soc Lond A Mater 2004;2048:2223–50.
[18] Monchoux R, Bourgoin M, Cartellier A. Analyzing preferential concentration and clustering of inertial particles in turbulence. Int J Multiphase Flow 2012;40:1–18.
[19] Monchoux R, Bourgoin M, Cartellier A. Preferential concentration of heavy particles: a Voronoi analysis. Phys Fluids 2010;22:10034.
[20] Marchioli C, Soldati A. Mechanisms for particle transfer and segregation in turbulent boundary layer. J Fluid Mech 2002;468:283–315.
[21] Lavezzo V, Soldati A, Geraschenko S, Warhaft Z, Collins LR. On the role of gravity and shear on inertial particle accelerations in near-wall turbulence. J Fluid Mech 2010;658:229–46.
[22] Marchioli C, Picciotto M, Soldati A. Particle dispersion and wall-dependent fluid scales in turbulent bounded flow: implications for local equilibrium models. J Turbul 2006;7:1–12.
[23] Germano M, Piomelli U, Moin P, Cabot WH. A dynamic subgrid-scale eddy viscosity model. Phys Fluids 1991;3:1760–5.
[24] Salvetti MV, Banerjee S. A-priori tests of a new dynamic subgrid-scale model for finite-difference large-eddy simulations. Phys Fluids 1995;7:2831–47.
[25] Marchioli C, Armenio V, Soldati A. Simple and accurate scheme for fluid velocity interpolation for Eulerian–Lagrangian computation of dispersed flows in 3D curvilinear grids. Comput Fluids 2007;36:1187–98.
[26] Cellino M, Lemmin U. Influence of coherent flow structures on the dynamics of suspended sediment transport in open-channel flow. J Hydraul Eng 2004;130:1077–88.
[27] Breugem WA, Uijttewaal WSJ. Sediment transport by coherent structures in a turbulent open channel flow experiment. In: Geurts BJ, Clercx HJH, Uijttewaal WSJ, editors. Particle-laden flow: from geophysical to Kolmogorov scales. Springer; 2007. p. 43–55.
[28] Nogichi K, Nezu I. Particle-turbulence interaction and local particle concentration in sediment-laden open-channel flows. J Hydro-Env Res 2009;3:54–68.
[29] Lelouvetel J, Bigillon F, Doppler D, Vinkovic I, Champagne JY. Experimental investigation of ejections and sweeps involved in particle suspension. Water Resour Res 2009;45:W02416.
[30] Chang YS, Scotti A. Turbulent convection of suspended sediments due to flow reversal. J Geophys Res 2006;111:C07001.
[31] Dubief Y, Delcayre F. On coherent-vortex identification in turbulence. J Turbul 2000;1:1–22.
[32] Konan NA, Kannengieser O, Simonin O. Stochastic modeling of the multiple rebound effects for particle-rough wall collisions. Int J Multiphase Flow 2009;35:933–45.
[33] Cuthbertson AJ, Ervine DA. Experimental study of fine sand particle settling in turbulent open channel flows over rough porous beds. J Hydraul Eng 2007;133:905–16.
[34] Kosinski P, Hoffmann AC. Extension of the hard-sphere particle-wall collision model to account for particle deposition. Phys Rev E 2009;79:061302.
[35] Reade WC, Collins LR. Effect of preferential concentration on turbulent collision rates. Phys Fluids 2000;12:2530–40.
[36] Jha SK, Bombardelli FA. Toward two-phase flow modeling of nondilute sediment transport in open channels. J Geophys Res Earth Surf 2010;115:F03015.
[37] Marchioli C, Salvetti MV, Soldati A. Appraisal of energy recovering sub-grid scale models for large-eddy simulation of turbulent dispersed flows. Acta Mech 2008;201:277–96.
[38] Kuerten JGM. Subgrid modeling in particle-laden channel flow. Phys Fluids 2006;18:025108.
[39] Shotorban B, Zhang KKQ, Mashayek F. Improvement of particle concentration prediction by defiltering. Int J Heat Mass Transf 2007;50:3728–39.
[40] Stolz P, Adams NA, Kleiser L. An approximate deconvolution model for large-eddy simulation with application to incompressible wall-bounded flows. Phys Fluids 2001;13:997–1015.
[41] Scotti A, Meneveau C. A fractal model for large eddy simulation of turbulent flow. Physica D 1999;127:198–232.
[42] Bianco F, Chibbaro S, Marchioli C, Salvetti MV, Soldati A. Intrinsic filtering errors of Lagrangian particle tracking in LES flow fields. Phys. Fluids 2012;24:045103.
[43] Piomelli U, Balaras E. Wall-layer models for large-eddy simulations. Ann Rev Fluid Mech 2002;34:349–74.
[44] Duprat C, Balarac G, Métais O, Congedo PM, Brugière O. A wall-layer model for large-eddy simulations of turbulent flows with/out pressure gradient. Phys Fluids 2011;23:015101.